NASA Technical Paper 2499

1985

An Update of the Total-Strain Version of SRP

James F. Saltsman
and Gary R. Halford

Lewis Research Center
Cleveland, Ohio

NASA
National Aeronautics
and Space Administration

Scientific and Technical Information Branch

Summary

An updated procedure has been developed for characterizing an alloy and predicting cyclic life by using the total-strain-range version of strainrange partitioning (TS-SRP). The principal feature of this update is a new procedure for determining the intercept of time-dependent elastic-strain-range-versus-cyclic-life lines. The procedure is based on an established relation between failure and the cyclic stress-strain response of an alloy. The stress-strain response is characterized by empirical equations presented in this report. These equations were determined with the aid of a cyclic constitutive model. The procedures presented herein reduce the testing required to characterize an alloy. Failure testing is done only in the high-strain, low-life regime; cyclic stress-strain response is determined from tests conducted in both the high- and low-strain regimes. These tests are carried out to stability of the stress-strain hysteresis loop but not to failure. Thus both the time and costs required to characterize an alloy are greatly reduced. This approach was evaluated and verified for two nickel-base superalloys, AF2-1DA and Inconel 718. The analyst can now predict cyclic life in the low-strain, long-life regime without having to conduct expensive failure tests in this regime or resort to questionable larger extrapolations.

Introduction

A total-strain-range version of strainrange partitioning (TS-SRP) has been introduced by Halford and Saltsman (ref. 1). This development, following the pioneering work of Manson and Zab (ref. 2), extends the capabilities of SRP into the low-strain, long-life regime, where the inelastic strains are small and difficult to determine by either experimental or analytical methods. In using the total-strain-range approach an alloy is characterized in much the same manner as for the original inelastic-strain-range version of SRP. Additional tests performed at the lower strain ranges would, of course, reduce extrapolation errors. However, since failure testing at the lower strain ranges is lengthy and expensive, it would be advantageous to find a way to characterize an alloy in the low-strain regime with a minimum of such tests. This issue is addressed by the present research.

TS-SRP requires the determination of the relation of the elastic strain range to life as well as the relation of the inelastic strain range to life. For cycles involving creep the elastic lines are influenced by hold time, wave shape, and how creep is introduced into the cycle (stress hold, strain hold, slow strain rate, etc.). Analysis shows that the elastic-strain-range-versus-life relations can be affected by flow response (i.e., the cyclic stress-strain-versus-hold-time response). Flow response can be determined by cycling a specimen until the stress-strain hysteresis loop approaches stability. These tests are much shorter and hence less expensive than failure tests.

Flow response for any conceivable cycle could be determined by using an appropriate constitutive flow model, provided that the constants are known for a material of interest. However, reliable and fully evaluated constitutive flow models are not presently available, particularly in the low-strain regime. This difficulty could be overcome if suitable empirical equations characterizing flow behavior were available. This concept has been successfully used by Brinkman et al. (ref. 3) for modeling the behavior of 2.25Cr-1Mo steel. Our initial efforts (ref. 1) showed that a considerable amount of flow data would be required to determine the relation between flow and failure behavior and thus the desired empirical relations. The limited amount of data generally available from failure testing was inadequate, and additional flow testing was no longer feasible after the original testing was completed. In searching for a solution to this dilemma of seemingly insufficient information, we propose using a combination of empiricism and constitutive theory.

Walker's functional theory (ref. 4) is available, and the computer program (ref. 5) for this theory has been recently made more efficient and user friendly. Although the Walker theory has been used herein, numerous other constitutive models developed over the past few years could be incorporated—such as the Robinson model (ref. 6). The Walker model was used to identify general trends in flow behavior, and we were able to develop empirical equations that describe these trends. These empirical equations make it easier to characterize the cyclic flow behavior of an alloy and to predict cyclic life in the low-strain, long-life regime at elevated temperature by using TS-SRP. To fully characterize the cyclic flow and failure of an alloy, failure testing is done in the high-strain, low-life regime according to the SRP guidelines of

Hirschberg and Halford (ref. 7). Flow behavior is documented along with failure behavior. And as a minimum requirement only flow testing is needed in the low-strain, long-life regime. This procedure greatly reduces the time and cost of characterizing the creep-fatigue behavior of alloys.

This report presents an updated procedure for characterizing an alloy and predicting cyclic life by using TS-SRP. The principal feature of this update is the method for determining the intercept of the time-dependent elastic-strain-range-versus-cyclic-life line. The procedure is based on an established relation between failure and the cyclic stress-strain response of an alloy. The stress-strain response is characterized by the empirical equations presented in this report.

Symbols

A general constant in empirical flow equations

A' general constant in empirical flow equations

B intercept of elastic-strain-range-versus-life relations

b power of cyclic life for elastic-strain-range-versus-life relations

C intercept of inelastic-strain-range-versus-life relations

C' intercept of equivalent inelastic line for combined creep-fatigue cycles

c power of cyclic life for inelastic-strain-range-versus-life relations

F strain fraction

K cyclic strain-hardening coefficient

m general power of time in empirical flow equations

N applied cycles or number of data points in prediction

n cyclic strain-hardening exponent

SE standard error of estimate

t hold time, sec

α power on total strain range in empirical flow equations

Δ range of variable

ϵ strain

σ stress

Subscripts:

c compression

cc creep strain in tension, creep strain in compression

cp creep strain in tension, plastic strain in compression

el elastic

f failure

in inelastic

ij pp,cc,pc,cp

obs observed

pc plastic strain in tension, creep strain in compression

pp plastic strain in tension, plastic strain in compression

pre predicted

t tension or total

Analysis

In the original version of TS-SRP (ref. 1) the time-dependent elastic line intercept (elastic strain range at $N_f = 1$) for cycles involving creep is obtained from an empirical equation with constants determined exclusively from failure data.

New developments have led to procedures that reduce the amount of failure testing required to characterize an alloy and to determine the elastic line intercept for creep-fatigue cycles. Analysis shows that flow behavior can be related to failure behavior in the following manner:

Failure behavior:

$$\Delta\epsilon_{el} = B(N_f)^b \tag{1}$$

$$\Delta\epsilon_{in} = C'(N_f)^c \tag{2}$$

where

$$C' = \left[\sum F_{ij}(C_{ij})^{1/c}\right]^c \tag{3}$$

Flow behavior:

$$\Delta\epsilon_{el} = K_{ij}(\Delta\epsilon_{in})^n \tag{4}$$

Our limited experience (ref. 1) suggests that the inelastic and elastic failure lines for creep-fatigue cycles can be assumed to be parallel to the corresponding failure lines for PP cycles, as shown in figure 1. It then follows that n in equation (4) is constant ($n = b/c$) for all wave shapes, as shown in figure 2. However, K_{ij} may well depend on how creep is introduced into the cycle (stress hold, strain hold, etc.). The time-dependent behavior of the elastic line for creep-fatigue cycles is shown in figure 3. Setting equation (1) equal to equation (4) and eliminating N_f by using equation (2), we obtain the following equation relating flow and failure characteristics:

$$B = K_{ij}(C')^n \tag{5}$$

In this equation the inelastic line intercepts C_{pp}, C_{cc}, C_{pc}, C_{cp}, and the exponent c are considered to be failure terms. The strain fractions F_{ij}, the cyclic strain-hardening coefficient K_{ij}, and the strain-hardening exponent n are considered to be flow terms. Thus the elastic line intercept B can be determined for a creep cycle from a combination of flow and failure data. Note that the cyclic strain-hardening coefficient and strain fractions will, in general, depend on waveform.

We are now in a position to establish a total-strain-range-versus-life relation and thus to predict life by using the TS-SRP approach. The total strain range is the sum of the elastic and inelastic strain ranges:

$$\Delta\epsilon_t = \Delta\epsilon_{el} + \Delta\epsilon_{in} \tag{6}$$

From equations (1) and (2) we obtain

$$\Delta\epsilon = B(N_f)^b + C'(N_f)^c \tag{7}$$

A schematic plot of equation (7) is shown in figure 1. Note that the solution of this equation gives the cyclic life for a theoretical zero-mean-stress condition. The final step in a life prediction is to adjust the computed life to account for any mean stress effects that may be present. In this report the method of mean stress correction proposed by Halford and Nachtigall (ref. 8) is used.

There are three basic variations of the general method for predicting life by using the TS-SRP approach, depending on what type of information is, or can be made, available.

Variant 1

(1) Determine the SRP inelastic-strain-range-versus-life relations and the PP elastic-strain-range-versus-life relation from failure tests. As an alternative the ductility-normalized SRP (DN-SRP) life relations proposed by Halford and Saltsman (ref. 9) could be used, but they do require plastic and creep ductility information at the temperature and failure times of interest.

(2) Calculate the cyclic strain-hardening coefficient K_{ij} and the strain fractions F_{ij} by using an appropriate constitutive flow model for which the material constants are known. If the DN-SRP life relations are used, the cyclic strain-hardening exponent n should be determined from tests and the slope of the PP elastic line calculated ($b = nc$).

(3) The elastic line intercept B can now be calculated by using equation (5) and the preceding information.

(4) Determine the total-strain-range-versus-life curve for the case in question (fig. 1). Enter the curve at the appropriate total strain range and determine cyclic life for the theoretical zero-mean-stress condition. In this report we have used the inversion method of Manson and Muralidharan (ref. 10) to solve equation (7). This life is then adjusted to account for mean stress effects according to reference 8.

Variant 2

(1) Determine inelastic-strain-range-versus-life relations and the PP elastic-strain-range-versus-life relation from failure tests.

(2) Determine the elastic line intercept B by using the empirical equation of Halford and Saltsman (ref. 1). The constants in this equation are determined from failure data. Failure tests should be performed at the lower strain ranges to reduce extrapolation errors.

(3) Measure strain ranges (elastic and inelastic) and stresses from failure tests and extrapolate to lower strain ranges by using empirical equations.

(4) Determine cyclic life by using step (4) of variant 1.

Variant 3

(1) Same as step (1) of variant 1.

(2) Conduct flow tests for creep-fatigue cycles of interest and obtain from these data necessary empirical correlations describing the flow behavior. If failure data are lacking and the DN-SRP life relations are used, tests must be done to determine the strain-hardening exponent n for PP cycles. The slope of the PP elastic line b can then be calculated ($b = nc$).

(3) Calculate the elastic line intercept B by using equation (5). The strain-hardening coefficient K_{ij} and the strain fractions F_{ij} are determined from the correlations obtained in step (2).

(4) Determine cyclic life by using step (4) of variant 1.

Although variant 1 is the most general procedure, it is not a viable option at this time because reliable constitutive flow models in the low-strain regime are not available. Variant 2 was used in our original TS-SRP paper (ref. 1) and relies on failure data for the determination of the required equation constants. Variant 3, the subject of the present paper, represents a middle ground between variants 1 and 2. Inelastic-strain-range-versus-life relations based on failure are necessary for reliable life predictions, but preliminary life predictions can be made by using the DN-SRP life relations and information obtained from flow tests.

Analysis Using Walker Model

The Walker constitutive model was used to generate the cyclic stress-strain or flow information needed to identify *trends* in the required SRP flow behavior. From this information we were able to obtain the required correlations, which are based on a simple power-law equation

$$y = A(t)^m \tag{8}$$

where y is the dependent variable representing several different variables, as discussed shortly, and t is the hold time per cycle. In this report t is the *total* hold time per cycle. Thus for CC cycles t is the sum of the hold times in both tension and compression. When dealing with CC cycles we have treated in the present paper only the case in which the cycles are balanced (i.e., PC or CP strain range components are negligibly small).

Generally A is a function of total strain range, as shown in figure 4. From the limited data available (ref. 1) the family of lines shown in figure 4 can be taken as parallel. Thus the exponent on time m is independent of total strain range. It was found that the intercept A can be correlated with total strain range by another power law, as shown in figure 5.

$$A = A'(\Delta\epsilon_t)^\alpha \tag{9}$$

thus

$$\frac{y}{(\Delta\epsilon_t)^\alpha} = A'(t)^m \tag{10}$$

As a result we can now normalize the dependent variable y and collapse the family of lines shown in figure 3 to a single line, as shown schematically in figure 6. The values of A', α, and m depend on the type of correlation and the mechanical properties of the alloy. Alloys with positive strain-rate-hardening characteristics soften under creep loading, and m will be negative for correlations when the dependent variable y is a stress or strain term. If an alloy hardens (i.e., negative strain rate hardening) under creep loading, m will be positive.

Several empirical correlations are used herein. The first two are used to determine the coefficients B and C' in equation (7). The remainder are used to determine the mean stress for use in the mean stress correction procedure.

K_{ij} vs hold time
F_{ij} vs hold time } To determine B and C'

$\Delta\epsilon_{el}$ vs hold time
$\Delta\sigma$ vs hold time
σ_c vs hold time
σ_t vs hold time } To determine mean stress correction

Note that each of these relations could be derived directly from a reliable, fully evaluated constitutive model were it available. Although the exact form of the relations would surely differ from that selected here, the trends would be similar.

Each type of correlation is discussed in the following sections. For a specific alloy these correlations depend on temperature, creep time, wave shape, and the manner in which creep is introduced into the cycle (stress hold, strain hold, etc.). Only two specific ways of introducing creep into a cycle have had to be considered in this report since these are the only types of waveforms for which data are available: stress hold and strain hold. These cycles are shown in figure 7.

Correlation Between Cyclic Strain-Hardening Coefficient and Hold Time

As noted in the previous section, the elastic-strain-range-versus-inelastic-strain-range flow relation for cycles involving creep (eq. (4)) is taken to be parallel to the PP line as shown in figure 2. The cyclic strain-hardening coefficient K_{ij} is shown as a function of hold time in figure 8. It is also dependent on temperature and wave shape:

$$K_{ij} = A(t)^m \tag{11}$$

In this relation the constant A is not a function of total strain range.

Correlation Between Elastic Strain Range and Hold Time

The general relation between elastic strain range and hold time is illustrated by the family of lines shown in figure 9. This family of lines collapses to a single line if the elastic strain range is divided by the total strain range raised to a suitable power:

$$\frac{\Delta\epsilon_{el}}{(\Delta\epsilon_t)^\alpha} = A'(t)^m \tag{12}$$

The constants in equation (12) can be determined from a regression analysis of the data obtained from the flow tests. A variation on this approach can be taken when insufficient data are available for a reliable curve fit to determine the values of A', α, and m in equation (12). This will generally be the case when analyzing existing sets of failure data.

Substituting $\Delta\epsilon_{el}$ from equation (4) into equation (12) yields

$$A'(\Delta\epsilon_t)^\alpha (t)^m = K_{ij}(\Delta\epsilon_{in})^n \tag{13}$$

Solving for $\Delta\epsilon_{in}$ gives

$$\Delta\epsilon_{in} = \beta(\Delta\epsilon_t)^{\alpha/n} \tag{14}$$

where

$$\beta = \left[\frac{A'(t)^m}{K_{ij}}\right]^{1/n} \tag{15}$$

Note that equation (14) is approximate and is used only to initially estimate α; it should not be used to calculate the inelastic strain range. We have found in the present study that the lines are approximately linear and parallel as indicated schematically in figure 10. Thus α/n can be estimated from a regression analysis by using equation (14). Since the value of the strain-hardening exponent n is usually known, the value of α can be estimated. Our experience indicates that PC and CP data can be combined for this type of correlation. This means that the value of α in equation (12) is the same for PC and CP cycles, provided that the creep strain is introduced into the cycle in the same manner (i.e., stress hold or strain hold).

The utility of this alternative approach is that it provides an initial estimate of α for analyzing the limited amount of data usually available in most data sources. Thus, with α known, the value of A' and m in equation (12) can be easily determined from a regression analysis of the data. The value of α may then be modified to obtain a better fit of the data. This approach is demonstrated in a later section.

Correlation Between Strain Fraction and Hold Time

The relation between strain fraction F_{ij} and hold time depends on wave shape and how creep is introduced into the cycle (i.e, stress hold or strain hold). For strain-hold cycles F_{ij} is influenced by total strain range as shown in figure 11. This relation can be reduced to a single line of the form of equation (10):

$$\frac{F_{ij}}{(\Delta\epsilon_t)^\alpha} = A'(t)^m \tag{16}$$

Calculations using the Walker constitutive model show that for stress-hold cycles the relation between F_{ij} and hold time is not influenced by total strain range. Thus for stress-hold cycles

$$F_{ij} = A'(t)^m \tag{17}$$

The values of α and m in equations (16) and (17) may be positive or negative depending on the type of cycle and the mechanical properties of the alloy.

Correlation Between Stress and Hold Time

Stress range versus hold time.—This correlation is not required for stress-hold cycles since for that special case the stress range is simply determined by multiplying the elastic-strain-range-versus-time correlation by Young's modulus. For strain-hold cycles, however, the power-law equation (eq. (10)) gives satisfactory results (fig. 12). The slope of this line may be positive or negative depending on the strain-rate-hardening characteristics of an alloy.

$$\frac{\Delta\sigma}{(\Delta\epsilon_t)^\alpha} = A'(t)^m \tag{18}$$

Maximum and minimum stress versus hold time.—A second stress correlation is required to determine the mean stress. For PC cycles (either strain or stress hold) the following correlation is used:

$$\frac{\sigma_c}{(\Delta\epsilon_t)^\alpha} = A'(t)^m \tag{19}$$

And for CP cycles (either stress or strain hold)

$$\frac{\sigma_t}{(\Delta\epsilon_t)^\alpha} = A'(t)^m \tag{20}$$

The mean stress and hence the mean stress effect on life can now be calculated by using the procedure of Halford and Nachtigall (ref. 8).

Evaluation of Method

The TS-SRP approach (variant 3) as presented herein has been applied to two nickel-base alloys, AF2-1DA and Inconel 718, by using literature data sources. These results feature fully reversed cycles with zero mean strain. Predictions made by the TS-SRP approach are compared with predictions made by using the inelastic-strain-range SRP approach. In the inelastic-strain-range approach strains, strain fractions, and mean stress are measured directly from test results. In the TS-SRP approach these values, along with the elastic line intercept, are calculated by using the various correlations.

Since separate flow tests were not conducted when the data on these two alloys were generated, we were unable to use fully the procedures of variant 3. Hence failure data were used to determine the empirical flow correlations.

AF2-1DA at 760 °C

Three data sources (refs. 8, 11, and 12) were available for this alloy, and each used a different heat of the alloy. All of the results reported in reference 8 were generated from stress-hold tests; those reported in reference 11 involved both stress- and strain-hold tests. The results

reported in reference 12 involve strain-hold tests and low-rate-strain-cycle (LRSC) tests. We assumed that the fatigue characteristics of the LRSC (PP + CC) waveform are similar to those of the balanced-cyclic-creep-rupture (BCCR) (PP + CC) waveform.

The first step in characterizing this alloy is to determine the four inelastic-strain-range-versus-life relations and the elastic-strain-range-versus-life relation for PP cycling, as shown in figures 13 and 14, respectively. We can now determine the empirical flow correlations for the PC, CP, and CC stress-hold cycles. The order in which this is done is not important, but we shall proceed in the same sequence as in the previous section.

The cyclic-strain-hardening-coefficient-versus-hold-time correlations were determined from equation (11). Individual values of K_{ij} were calculated from equation (4) and the value of n (0.173) shown in figure 15. The results of the regression analyses of these data are shown in figure 16. The negative slope indicates that the alloy exhibited a small degree of cyclic strain rate softening.

The elastic-strain-range-versus-hold-time correlations were determined from equation (12). The six PC, three CP, and three CC points available were considered to be inadequate for a reliable estimate of the constants in equation (12). Thus we used equation (14) to obtain an initial estimate of α. Because of the limited amount of data, this still may not be the best value of α. The inelastic-strain-range-versus-total-strain-range data are shown in figure 17. Results to date indicate that the PC and CP data can be combined for this type of plot.

For the exponent values from figure 17 and equation (14) the initial estimates of α were 0.62 for PC and CP cycles and 0.53 for CC cycles. Note that these values of α are only for the elastic-strain-range-versus-hold-time correlations. We found in our analysis that the goodness of fit as measured by the correlation coefficient generally increased to some maximum value with increasing α and then decreased as α continued to increase. The best values of α were thus found by trial and error by using these values as initial estimates. For PC cycles the best value for α was 0.70, which is reasonably close to the initially estimated value (0.62). Since there were six PC data points and only three each for the CP and CC cycles, we assumed $\alpha = 0.70$ for all types of cycles. The elastic-strain-range-versus-hold-time correlations could then be determined and are shown in figure 18.

The strain-fraction-versus-hold-time correlations were obtained by using equation (17) and are shown in figure 19. Note that for the stress-hold waveform the constant A' in equation (16) is not a function of total strain range.

The stress-versus-hold-time correlations are used to calculate the mean stress effects. They were obtained by using equations (18), (19), and (20) and are shown in figure 20. In this paper stress is in units of megapascals (MPa). As noted in the previous section a separate stress-range-versus-hold-time correlation is not needed for stress-hold cycles; it is determined by multiplying the elastic strain range correlation by Young's modulus.

We now had all of the equations necessary to predict cyclic life of stress-hold cycles for AF2-1DA at 760 °C by using the TS-SRP approach. The predictive ability of this approach was evaluated by comparing the results with predictions made with the inelastic-strain-range SRP approach. All of the data in reference 8 were used to determine these correlations. Thus by "predicting" these data, we obtained a measure of our ability to correlate the data. These "predictions" and those based on the inelastic-strain-range approach are shown in figure 21. The degree of fit is summarized in tables inset in the figures. These results are nearly identical as measured by the standard error of estimate (SE).

The standard error of estimate used to quantify the accuracy of the predictions is given by the following equation:

$$SE = \left(\frac{\sum [\log(N_{obs}) - \log(N_{pre})]^2}{N} \right)^{1/2} \tag{21}$$

This equation can also be written in the following form:

$$SE = \left\{ \frac{\sum \left[\log\left(\frac{N_{obs}}{N_{pre}} \right) \right]^2}{N} \right\}^{1/2} \tag{22}$$

From this form it is apparent that the standard error of estimate is the root mean square of the ratio of observed life to predicted life. The advantage of determining the standard error of estimate in this manner is that its value is determined by the ratio of the lives. It is not affected by the actual values of the lives. Thus it is possible to directly compare results from the analyses of various data sources.

Life predictions for the stress-hold tests reported in reference 11 and the LRSC tests reported in reference 12 are shown in figure 22. The TS-SRP approach predicted the data in reference 11 even better than the inelastic-strain-range SRP approach. The reverse was true for the LRSC (solid symbols). The assumption that LRSC data can be predicted by using stress-hold correlations may not be accurate enough. Note that the stress-hold data and the LRSC data used here were obtained from two different heats of the alloy. Overall the predictions made with the TS-SRP approach were slightly better than those made with the inelastic-strain-range SRP approach as measured by the standard error of estimate.

The correlations for strain-hold cycles were determined by using the appropriate data from reference 11. These correlations are shown in figures 23 to 27; life "predictions" for these data are shown in figure 28. The life predictions using the total- and inelastic-strain-range SRP approaches were quite similar except for the two PC points in figure 28(a). For these two points the calculated elastic strain range was greater than the total strain range. Obviously this could not be correct and was due to uncertainties in the correlations. To avoid this dilemma, the calculated elastic strain range was restricted to not exceed the known total strain range.

Life predictions of the independent strain-hold data in reference 12 are shown in figure 29. The predictions based on the TS-SRP approach are comparable to those based on the inelastic-strain-range approach.

Inconel 718 at 650 °C

Two data sources (refs. 11 and 13) were available for this alloy, and both featured the strain-hold waveform only. The data reported in reference 11 were obtained from specimens from bar stock, and the creep-fatigue data in reference 13 were obtained from three heats (heats 1, 2, and 6) of the alloy in plate form. Information on the heat treatment of heats 1, 2, and 6 is given in references 13 and 14. The different processing histories can be expected to produce different mechanical properties.

Heat 6 of reference 13, chosen as the reference heat because of its completeness, was used to establish the life relations and the flow correlations required for TS-SRP life predictions (figs. 30 to 37). Life "predictions" of these data are shown in figure 38 for both the total- and original inelastic-strain-range versions of SRP. The predictions made by using the TS-SRP approach were slightly better as measured by the standard error of estimate.

Life predictions for heats 1 and 2 of reference 13 are shown in figure 39. The predictions based on the TS-SRP approach were nearly identical to those based on the inelastic-strain-range approach as measured by the standard error of estimate. These predictions included six LRSC tests (indicated by the solid symbols). Previously for alloy AF2-1DA we assumed that this type of cycle could be predicted by using stress-hold flow correlations. Here we assumed that strain-hold correlations could be used. This was done because more appropriate correlations simply were not available. Our experience indicates that correlations for one type of waveform (stress hold, say) may be used to predict the lives of strain-hold cycles provided that the cycle types are the same (PC, CP, or CC). The accuracy of the predictions will suffer accordingly, but waveform effects should be less at the lower strain ranges.

Life predictions for the data in reference 11 are shown in figure 40. Both methods overpredicted the data. Examination of the data shows that the flow behavior was similar to that of the reference heat, but it was less fatigue resistant.

The results of these predictions for the two alloys were encouraging and strongly suggested that the method of determining the elastic line intercept B is sound. However, a more direct verification of equation (5) is highly desirable. Equation (5) was derived on the assumption that the inelastic- and elastic-strain-range failure lines for PC, CP, and CC cycles are parallel to the corresponding lines for PP cycles. This assumption implies that the strain-hardening exponent n in equation (4) is constant for all cycles. This value is determined from PP data or from rapid-cycling flow tests.

The validity of these assumptions and the ability of equation (5) to calculate the elastic line intercept can be evaluated by comparing these "calculated" values against "observed" values determined from test data.

The observed values of B were determined from the reported values of elastic strain range and the observed cyclic life.

$$B = \frac{\Delta\epsilon_{el}}{(N_f)^b} \tag{23}$$

Note that the observed life is for the theoretical zero-mean-stress condition. The results of these calculations are shown in figure 41. The results were generally good and indicated that equation (5) is valid. The "factor of 2" lines in figure 41 indicate the extent to which the elastic line intercept can vary when life is calculated on an elastic basis.

Concluding Remarks

An updated total-strain-range version of strainrange partitioning (TS-SRP) has been developed that makes it easier to characterize an alloy in the low-strain regime. This was accomplished by developing a set of empirical equations that characterize the constitutive behavior of an alloy. The constants in these equations can be determined from flow test results alone. Data from failure tests are not required. For a given alloy these equations are a function of temperature, wave shape (PC, CP, CC), and the method of introducing creep into a cycle (stress hold or strain hold, etc.).

To fully characterize an alloy, failure tests are conducted in the high-strain-range regime, where test times and costs are reasonable. The data from these tests are used to determine the inelastic-strain-range-versus-life relations and the elastic-strain-range-versus-life relation for the pure fatigue case of PP cycling. Flow testing is then done in the low-strain regime, where

failure testing would be prohibitively expensive. These data are used to determine the constants in the empirical constitutive flow equations.

The analyst now has sufficient information to predict the life of a cycle of interest. In our original total-strain-range SRP paper (ref. 1), the elastic line intercept was calculated by using an empirical equation with constants determined from failure data alone. The updated version presented herein is expected to reduce extrapolation errors in the determination of the elastic line intercept because the flow tests can be conducted at lower strain ranges than failure tests.

References

1. Halford, G.R.; and Saltsman, J.F.: Strainrange Partitioning—A Total Strain Version, International Conference on Advances in Life Prediction Methods. ASME, New York, 1983, pp. 17-26.
2. Manson, S.S.; and Zab, R.: Treatment of Low Strains and Long Hold Times in High Temperature Metal Fatigue by Strainrange Partitioning. ORNL/Sub-3988/1, Case Western Reserve Univ., Cleveland, Ohio, 1977.
3. Brinkman, C.R.; Strizak J.P.; and Booker, M.K.: Experiences in the Use of Strainrange Partitioning for Predicting Time Dependent Strain-Controlled Cyclic Lifetimes of Uniaxial Specimens of 2¼ Cr-1Mo Steel, Type 316 Stainless Steel, and Hastelloy X. Characterization of Low Cycle High Temperature Fatigue by the Strainrange Partitioning Method, AGARD CP-243, AGARD, Paris, France, 1978, pp. 15-1 to 15-18.
4. Walker, K.P.: Research and Development Program for Nonlinear Structural Modeling with Advanced Time-Temperature Dependent Constitutive Relationships. (PWA-5700-5) United Technologies Research Center; (NASA Contract NAS3-22055) NASA CR-165533, 1981.
5. Chang, T.Y.; and Thompson, R.L.: A Computer Program for Predicting Nonlinear Uniaxial Material Responses Using Viscoplastic Models. NASA TM-83675, 1984.
6. Robinson, D.N.; and Swindeman, R W.: Unified Creep-Plasticity Constitutive Equations for 2¼Cr-1Mo Steel at Elevated Temperature. ORNL/TM-8444, 1982.
7. Hirschberg, M.H.; and Halford, G.R.: Use of Strainrange Partitioning to Predict High-Temperature Low-Cycle Fatigue Life. NASA TN D-8072, 1976.
8. Halford, G.R.; and Nachtigall, A.J.: Strainrange Partitioning Behavior of an Advanced Gas Turbine Alloy, AF2-1DA, J. Aircr., vol. 17, no. 8, Aug. 1980, pp. 598-604.
9. Halford, G.R.; Saltsman, J.F.; and Hirschberg, M.H.: Ductility-Normalized Strainrange Partitioning Life Relations for Creep-Fatigue Life Prediction. Environmental Degradation of Engineering Materials, Virginia Polytechnic Institute and State Univ., Blacksburg, VA. 1977, pp. 599-612.
10. Manson, S.S.; and Muralidharan, U.: A Single-Expression Formula for Inverting Strain-Life and Stress-Strain Relationships, NASA CR-165347, 1981.
11. Thakker, A.B.; and Cowles, B.A.: Low Strain, Long Life Creep Fatigue of AF2-1DA and INCO 718. (FR-15656, Pratt & Whitney Aircraft; NASA Contract NAS3-22387.), NASA CR-167989, 1983.
12. Hyzak, J.M.; The Effects of Defects on the Fatigue Initiation Process in Two P/M Super Alloys. AFWAL-TR-80-4063, 1980. (AD-A093509.)
13. Korth, G.E.; and Smolik, G.R.: Physical and Mechanical Test Data of Alloy 718. TREE-1254, Idaho National Engineering Lab, Idaho Falls, ID, 1978.
14. Brinkman, C.R.; and Korth, G.E.: Strain Fatigue and Tensile Behavior of Inconel 718 from Room Temperature to 650 °C, J. Test. Eval.,vol. 2, no. 4, July 1974, pp. 249-259.

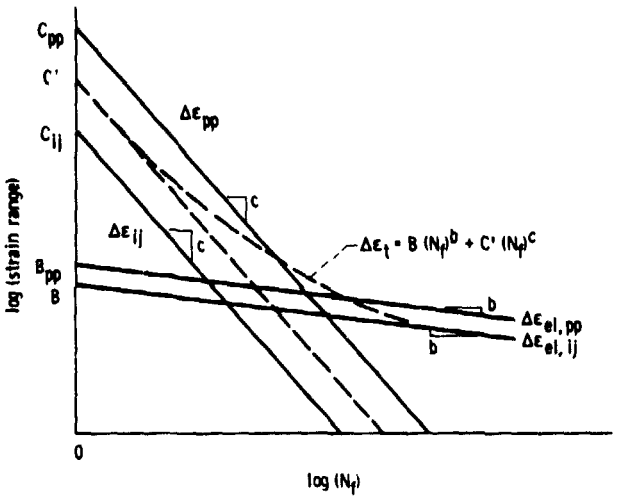

Figure 1.—Relation between total strain range and life for creep-fatigue cycles. Inelastic line intercept C' is determined from equation (3) and elastic line intercept B is determined from equation (5).

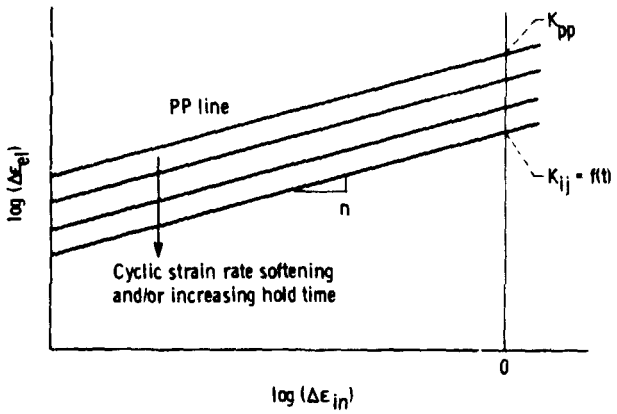

Figure 2.—Relation between inelastic and elastic strain ranges for creep-fatigue cycles. Cyclic strain-hardening coeffi ent K_{ij} is a function of hold time and strain-rate-hardening characteristics of an alloy.

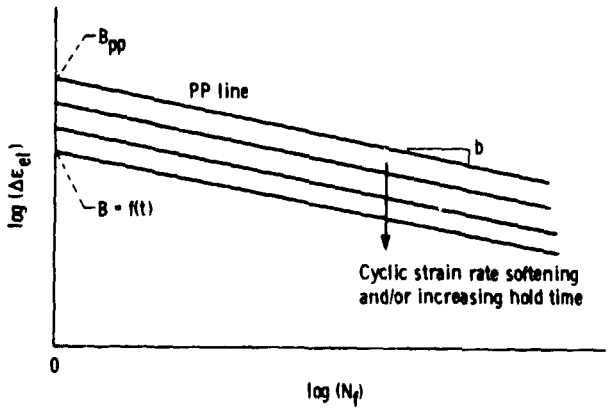

Figure 3.—Relation between elastic strain range and life for creep-fatigue cycles. Variation in elastic line intercept is a function of hold time and strain-rate-hardening characteristics of an alloy.

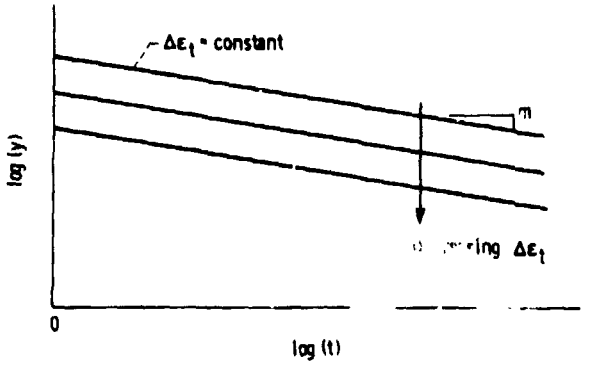

Figure 4.—Power-law relation used to correlate flow data. Lines are parallel, and intercept A at $t = 1$ sec is a function of total strain range.

Figure 5.—Relation between intercept of power-law equation and total strain range.

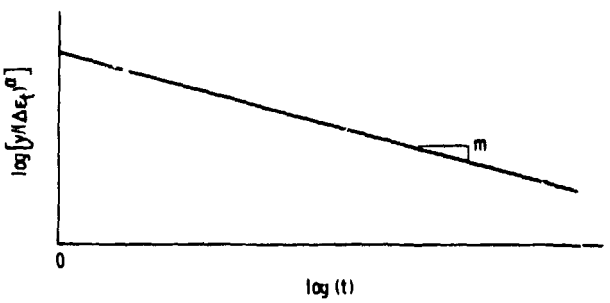

Figure 6.—Power law normalized on total strain range raised to suitable power, eliminating family of lines shown in figure 4.

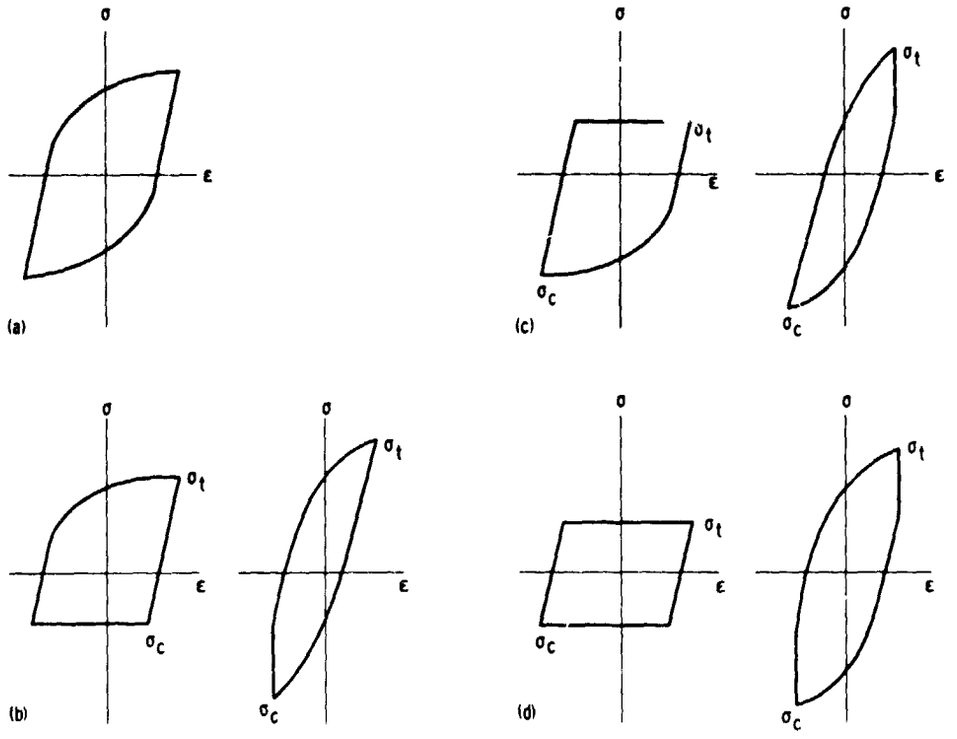

(a) PP cycle. (c) CP cycle.
(b) PC cycle. (d) CC cycle.

Figure 7.—Generic SRP wave shapes used in this report.

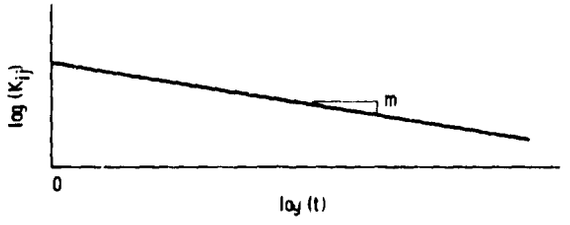

Figure 8.—Relation between cyclic strain-hardening coefficient K_{ij} and hold time for creep-fatigue cycles. Slope is negative for alloys exhibiting cyclic strain rate softening and positive for alloys exhibiting cyclic strain rate hardening.

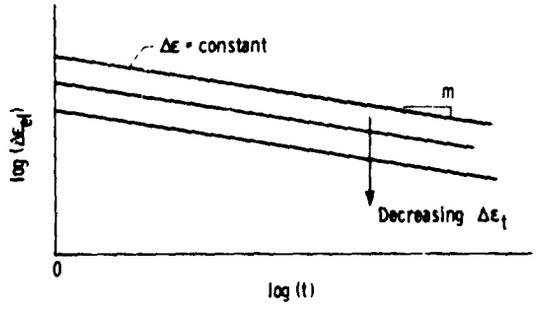

Figure 9.—Relation between elastic strain range and hold time. Slope is negative for alloys exhibiting cyclic strain rate softening and positive for alloys exhibiting cyclic strain rate hardening.

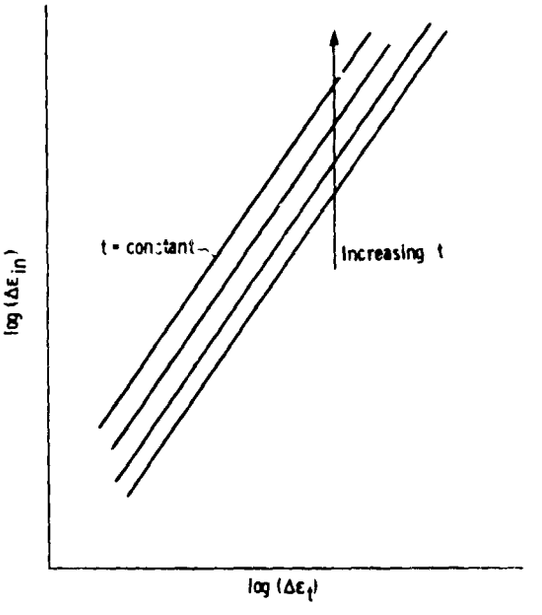

Figure 10.—Relation between total and inelastic strain ranges.

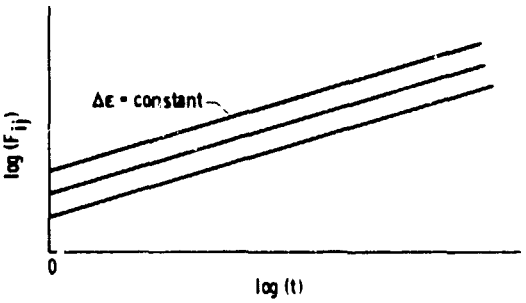

Figure 11.—Relation between strain fraction F_{ij} and hold time.

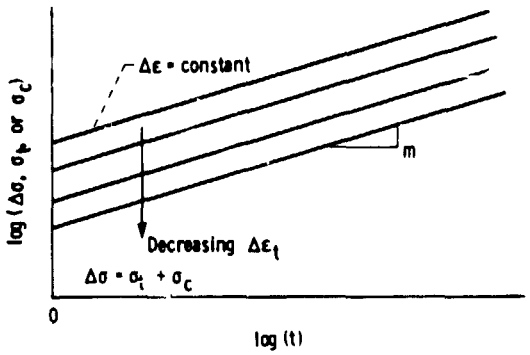

Figure 12.—Relation between stress and hold time for creep-fatigue cycles. Slope of lines may be positive or negative.

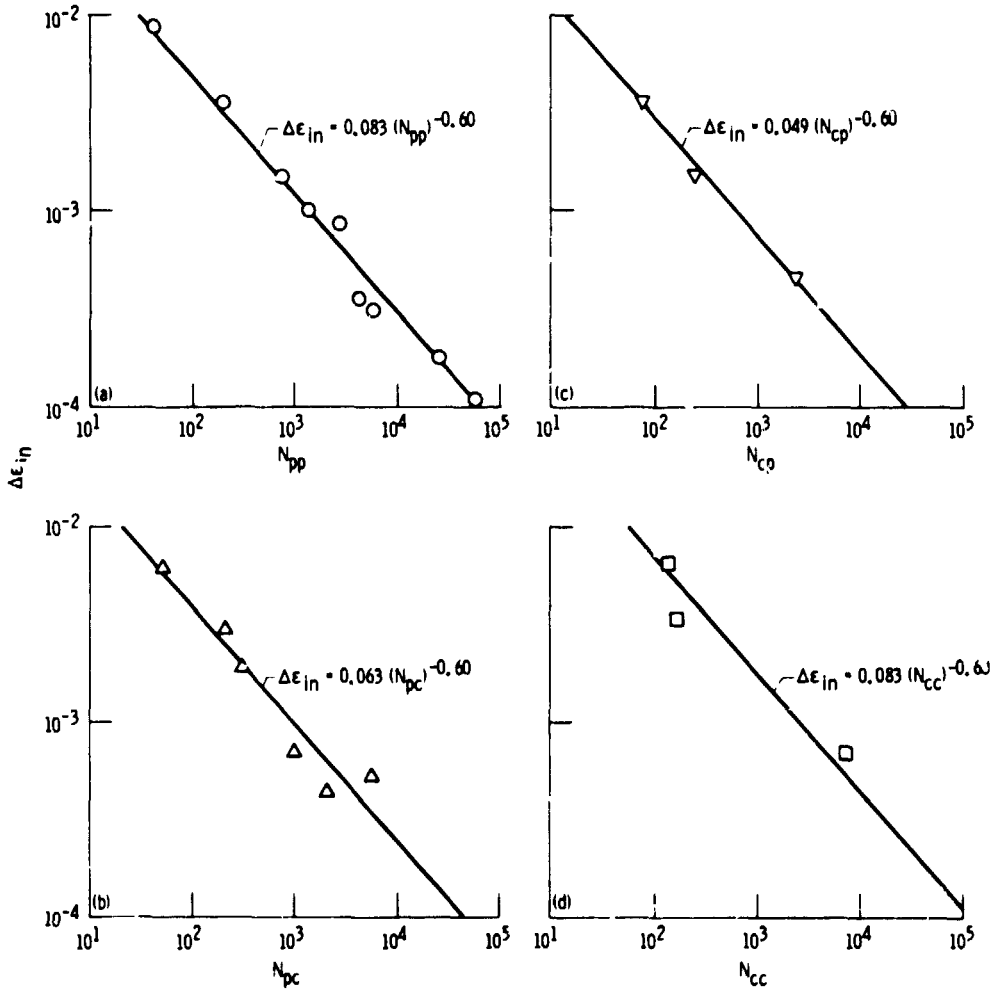

(a) PP correlation. (b) PC correlation.
(c) CP correlation. (d) CC correlation.

Figure 13.—Relation between inelastic strain range and life for zero-mean-stress condition: alloy, AF2-1DA; temperature, 760 °C. (Data from ref. 8.)

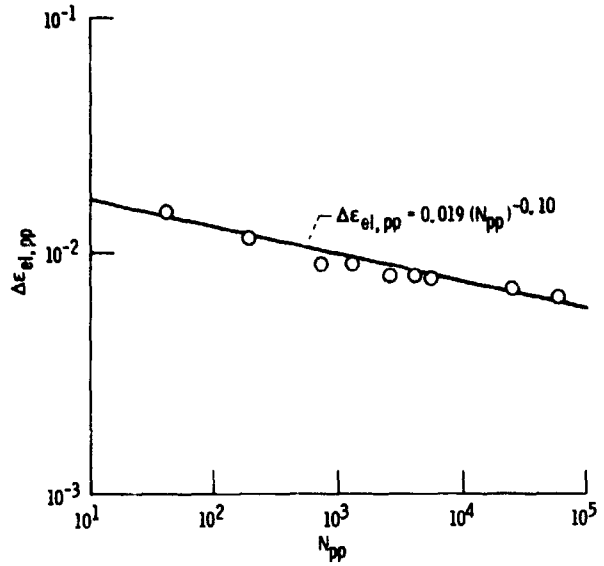

Figure 14.—Relation between elastic strain range and life for PP cycles: alloy, AF2-1DA; temperature, 760 °C. (Data from ref. 8.)

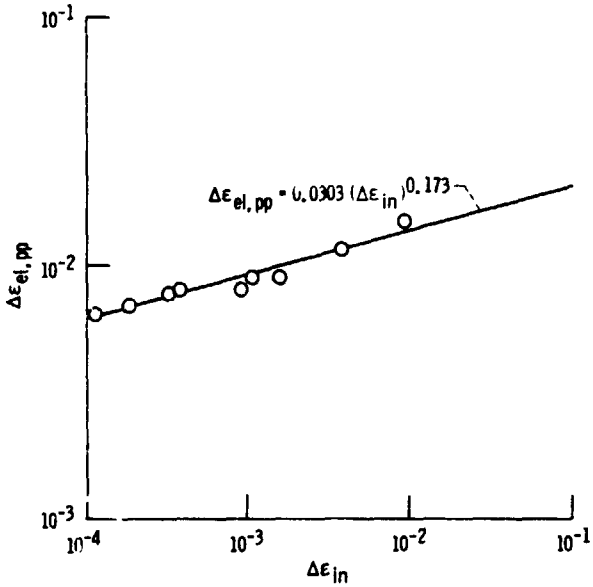

Figure 15.—Relation between elastic and inelastic strain range for PP cycles: alloy, AF2-1DA; temperature, 760 °C. (Data from ref. 8.)

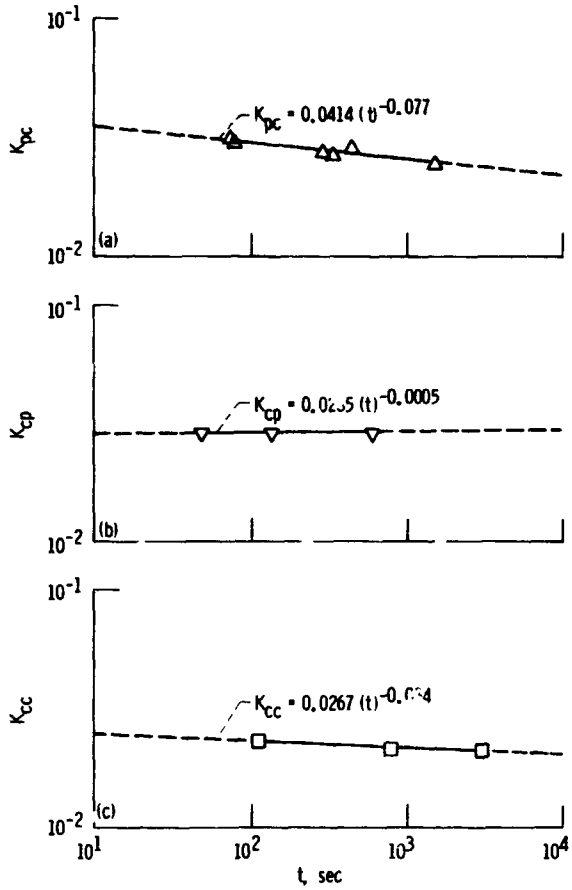

(a) PC correlation.
(b) CP correlation.
(c) CC correlation.

Figure 16.—Relation between cyclic strain-hardening coefficient and hold time for stress-hold cycles: alloy, AF2-1DA; temperature, 760 °C. (Data from ref. 8.)

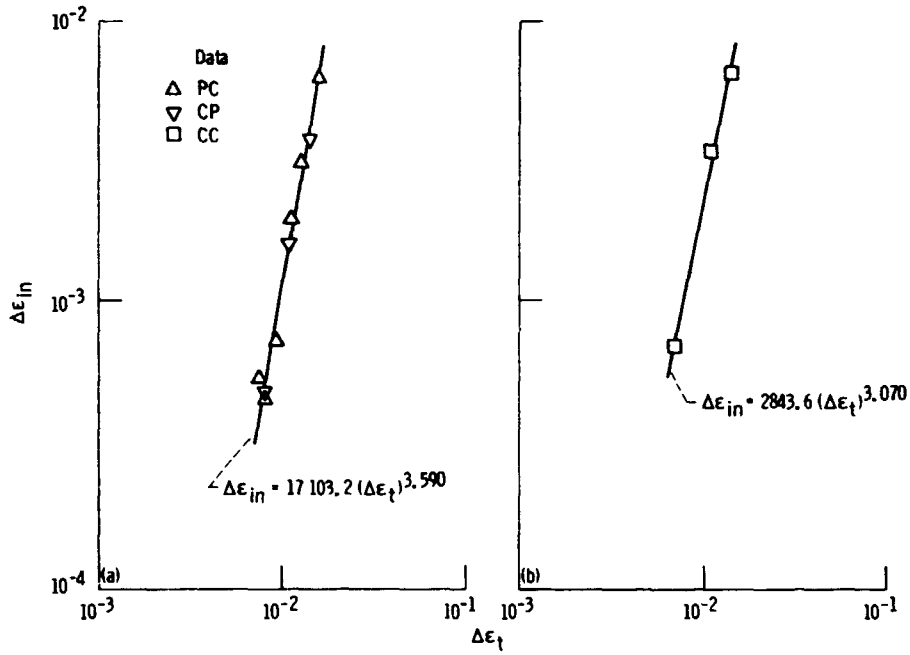

(a) PC and CP data.
(b) CC data.

Figure 17.—Relation between total and inelastic strain ranges for stress-hold cycles: alloy, AF2-1DA; temperature, 760 °C. (Data from ref. 8.)

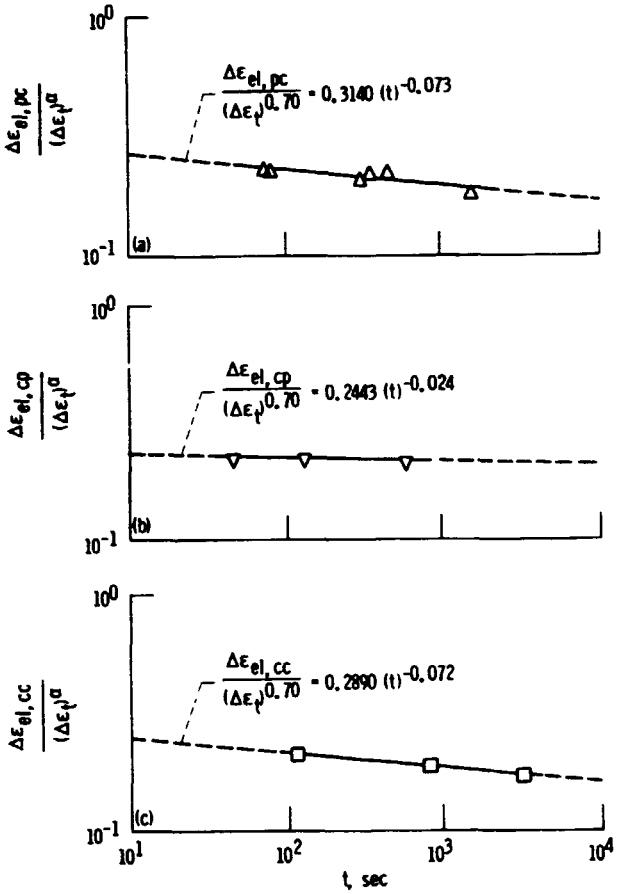

(a) PC correlation.
(b) CP correlation.
(c) CC correlation.

Figure 18.—Relation between elastic strain range and hold time for stress-hold cycles: alloy, AF2-1DA; temperature, 760 °C. (Data from ref. 8.)

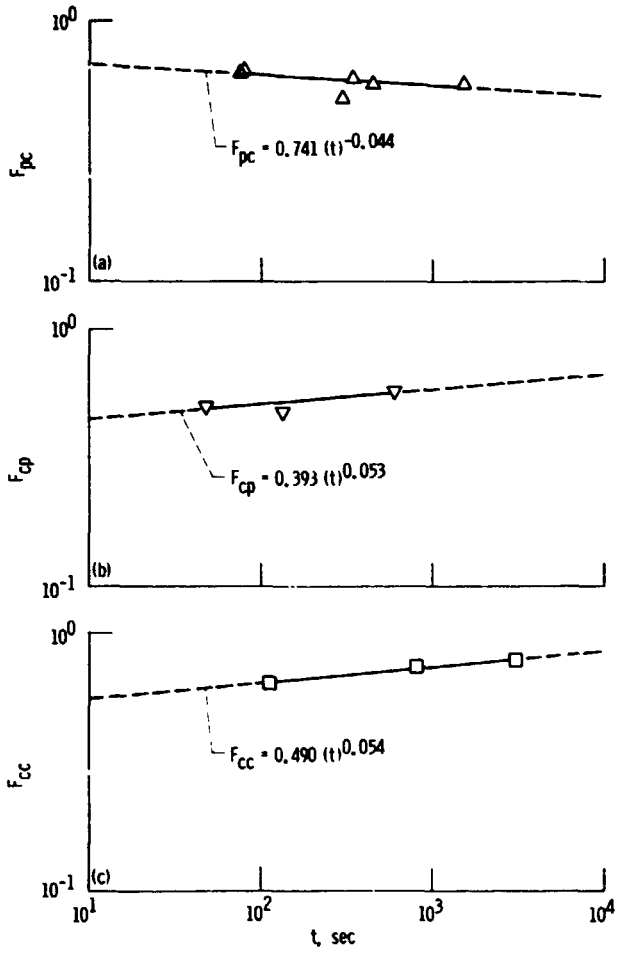

(a) PC correlation.
(b) CP correlation.
(c) CC correlation.

Figure 19.—Relation between strain fraction and hold time for stress-hold cycles: alloy, AF2-1DA; temperature, 760 °C. (Data from ref. 8.)

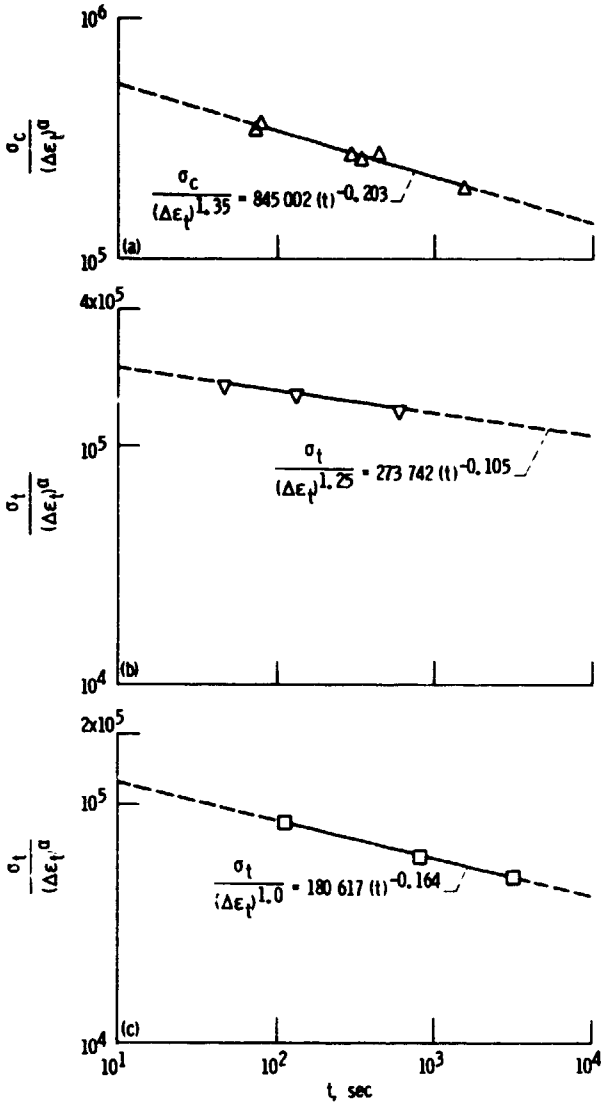

(a) PC correlation.
(b) CP correlation.
(c) CC correlation.

Figure 20.—Relation between stress and hold time for stress-hold cycles: alloy, AF2-1DA; temperature, 760 °C. (Data from ref. 8.)

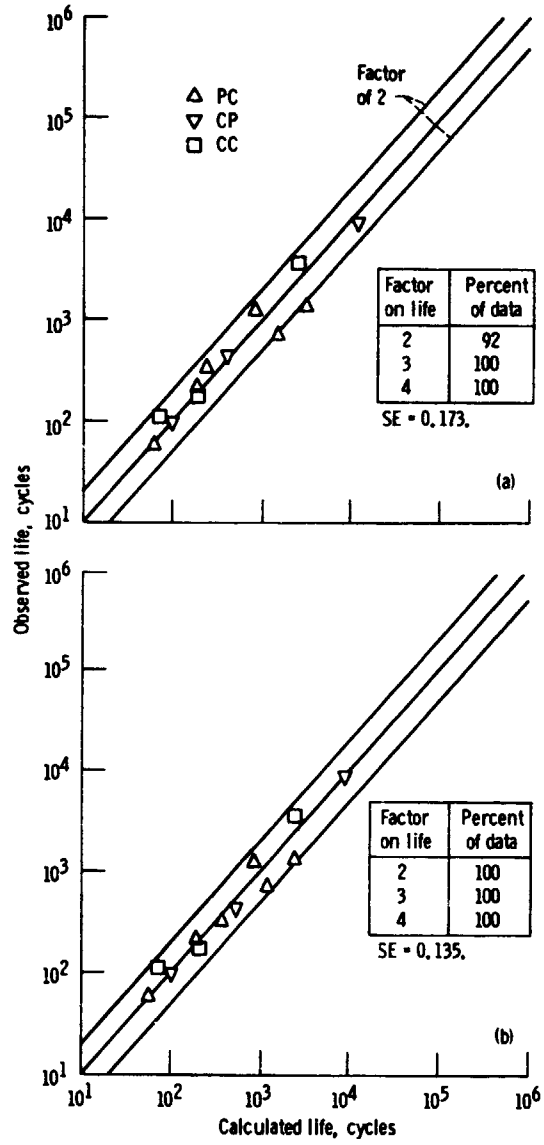

(a) Total-strain-range approach.
(b) Inelastic-strain-range approach.

Figure 21.—Life "predictions" of data used to establish stress-hold correlations: alloy, AF2-1DA; temperature, 760 °C. (Data from ref. 8.)

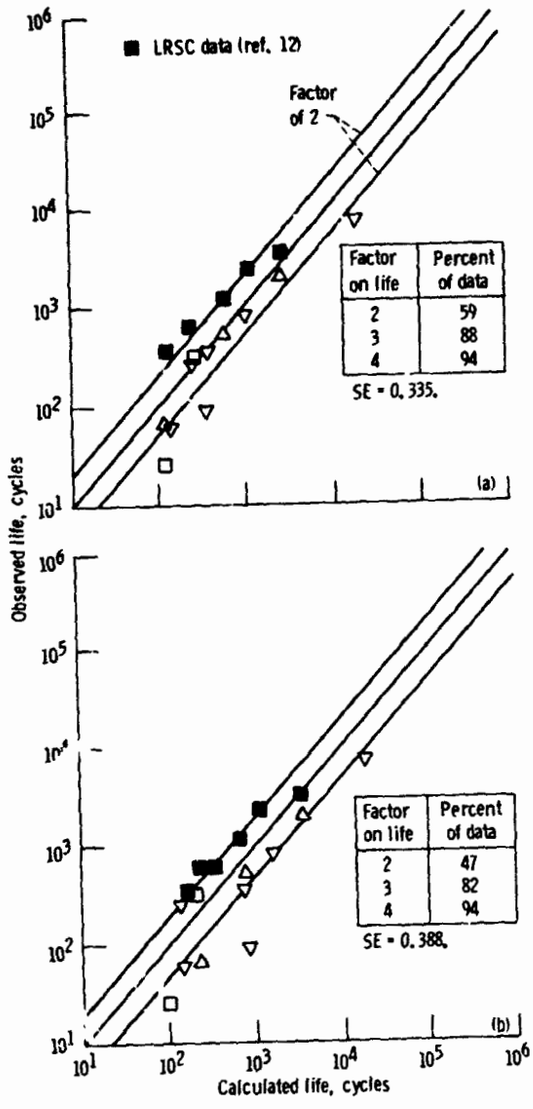

(a) Total-strain-range approach.
(b) Inelastic-strain-range approach.

Figure 22.—Life predictions of stress-hold data from reference 11 and low-rate strain cycle data from reference 12: alloy, AF2-1DA; temperature, 750 °C.

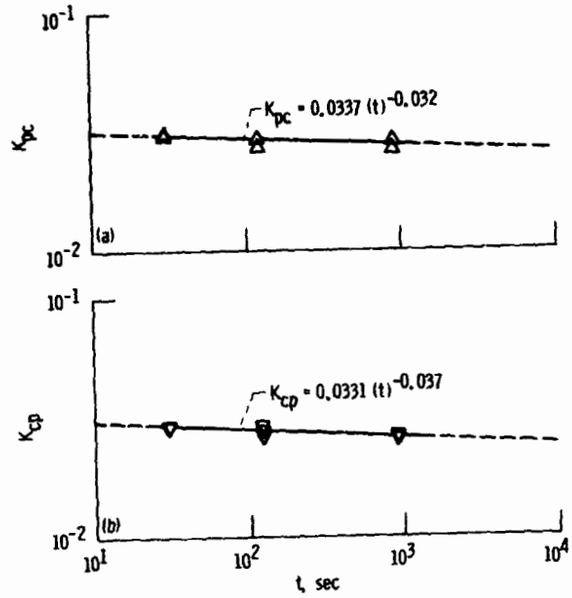

(a) PC correlation
(b) CP correlation.

Figure 23.—Relation between cyclic strain-hardening coefficient and hold time for strain-hold cyclic: alloy, AF2-1DA; temperature, 760 °C. (Data from ref. 11.)

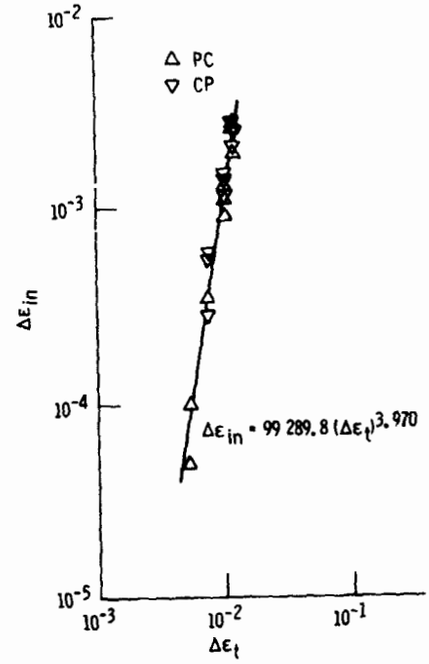

Figure 24.—Relation between total and inelastic strain ranges for strain-hold cycles with PC and CP data combined: alloy, AF2-1DA; temperature, 760 °C. (Data from ref. 11.)

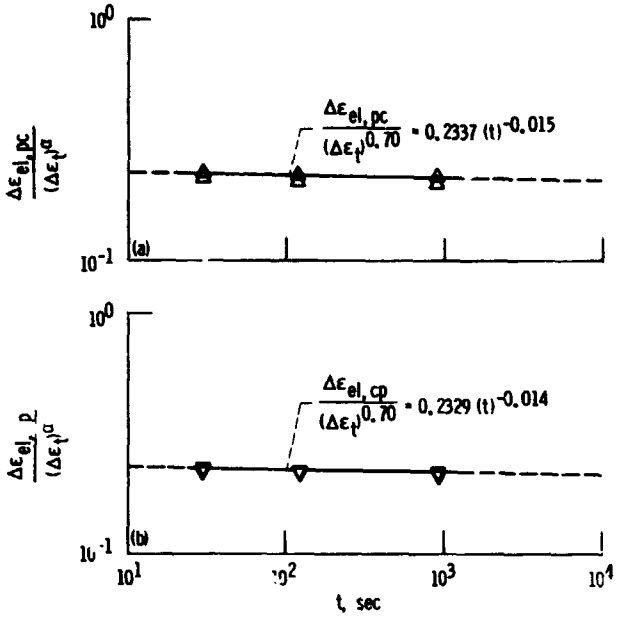

(a) PC correlation.
(b) CP correlation.

Figure 25.—Relation between elastic strain range and hold time for strain-hold cycles: alloy, AF2-1DA; temperature, 760 °C. (Data from ref. 11.)

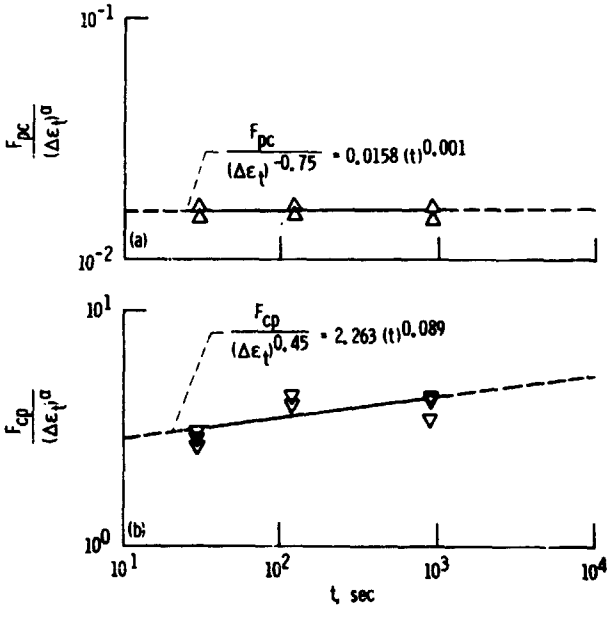

(a) PC correlation.
(b) CP correlation.

Figure 26.—Relation between strain fraction and hold time for strain-hold cycles: alloy, AF2-1DA; temperature, 760 °C. (Data from ref. 11.)

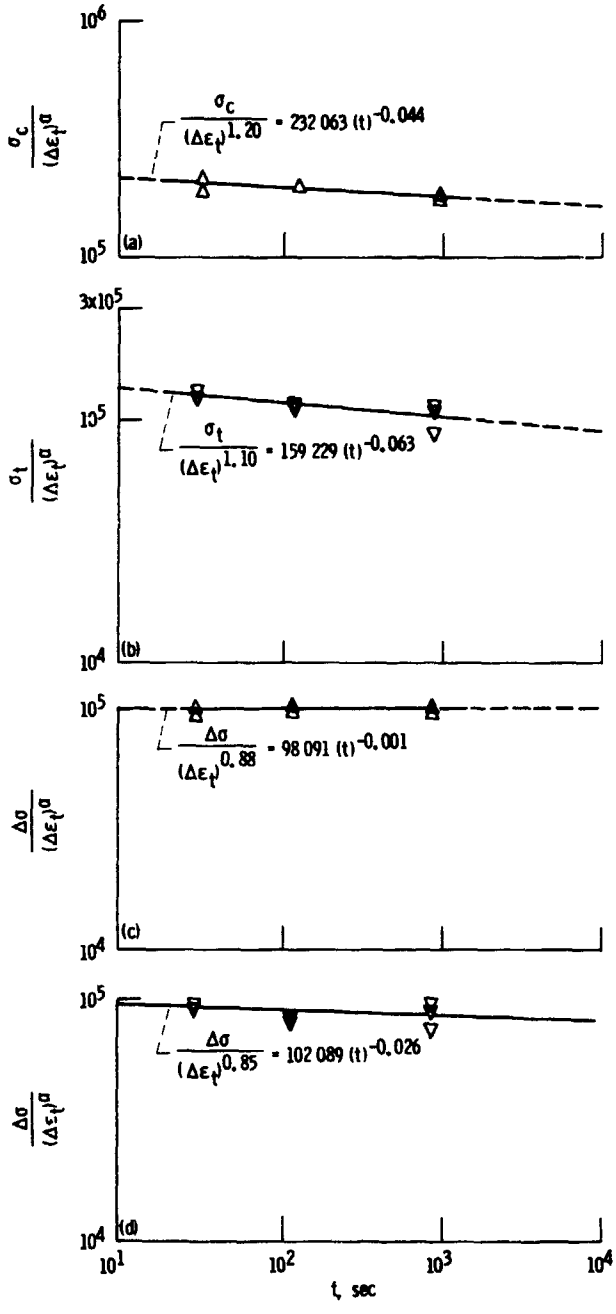

(a) PC correlation, compressive stress.
(b) CP correlation, tensile stress.
(c) PC correlation, stress range.
(d) CP correlation, stress range.

Figure 27.—Relation between stress and hold time for strain-hold cycles. (Data from ref. 11.)

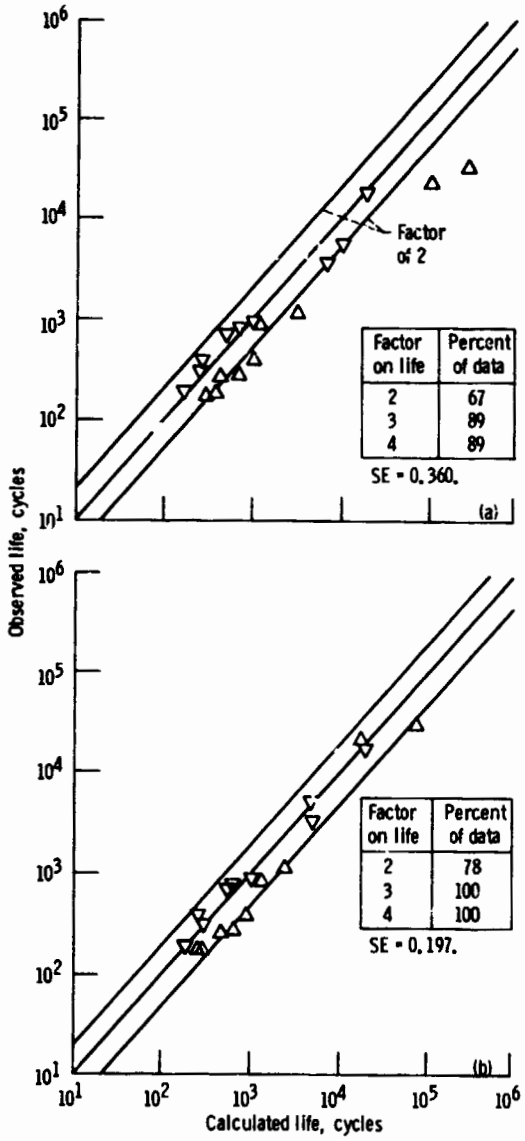

(a) Total-strain-range approach.
(b) Inelastic-strain-range approach.

Figure 28.—Life "predictions" of data used to establish strain-hold relations: alloy, AF2-1DA; temperature, 760 °C. (Data from ref. 11.)

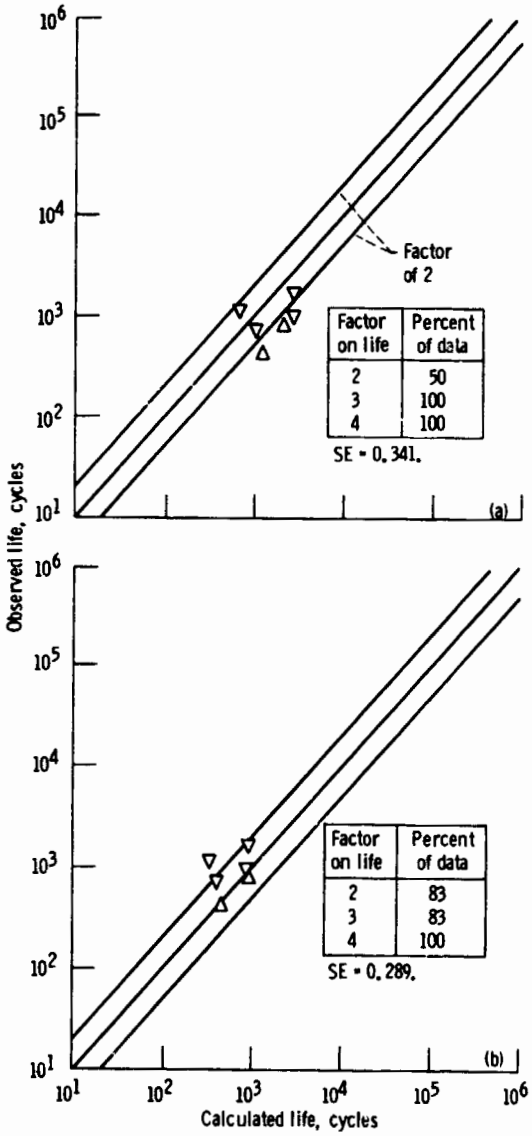

(a) Total-strain-range approach.
(b) Inelastic-strain-range approach.

Figure 29.—Life predictons of strain-hold data from reference 12: alloy, AF2-1DA; temperature, 760 °C.

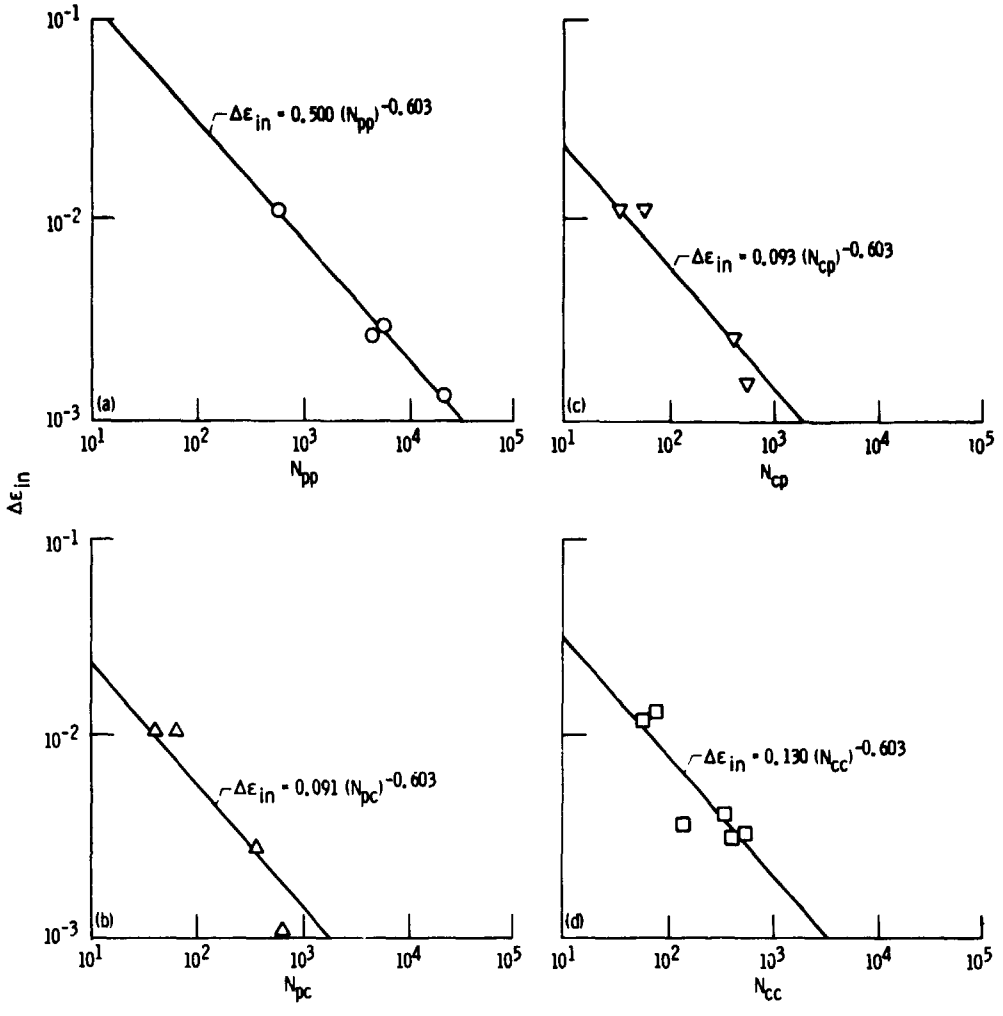

(a) PP correlation. (c) CP correlation.
(b) PC correlation. (d) CC correlation.

Figure 30.—Relation between inelastic strain range and life for zero-mean-stress condition: alloy, Inconel 718; temperature, 650 °C. (Data from ref. 13, heat 6.)

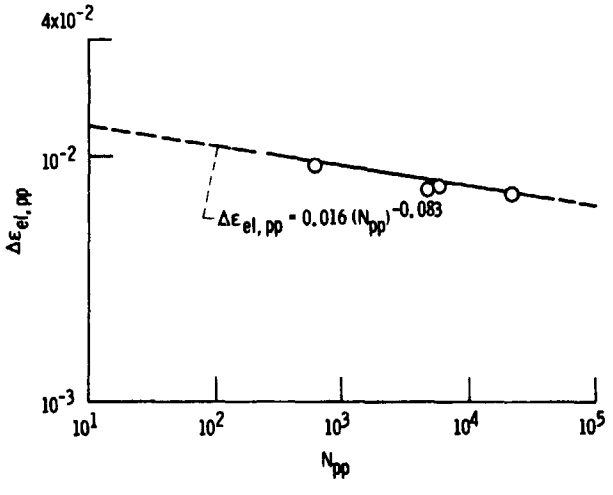

Figure 31.—Relation between elastic strain range and life for PP cycles and zero-mean-stress condition: alloy, Inconel 718; temperature, 650 °C. (Data from ref. 13, heat 6.)

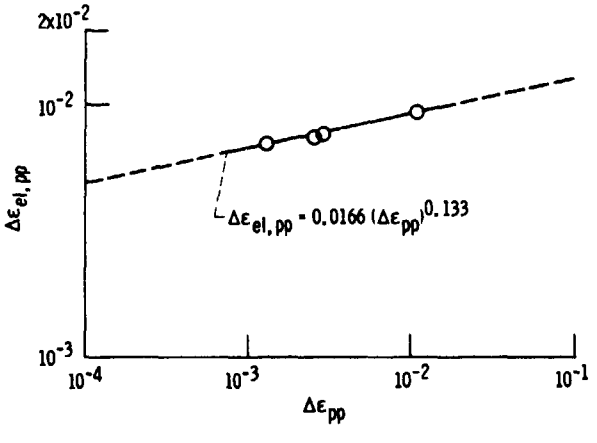

Figure 32.—Relation between elastic and inelastic strain ranges for PP cycles: alloy, Inconel 718; temperature, 650 °C. (Data from ref. 13, heat 6.)

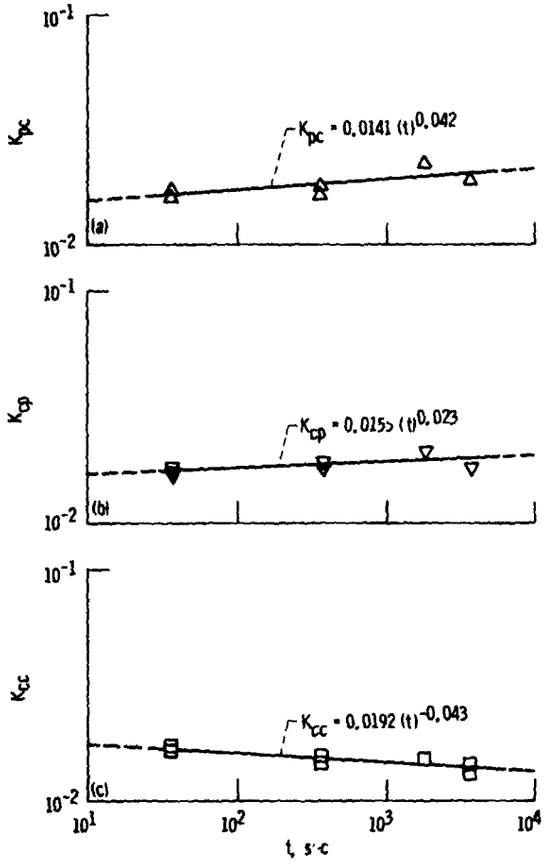

(a) PC correlation.
(b) CP correlation.
(c) CC correlation.

Figure 33.—Relation between cyclic strain-hardening coefficient and hold time for strain-hold cycles: alloy, Inconel 718; temperature, 650 °C. (Data from ref. 13, heat 6.)

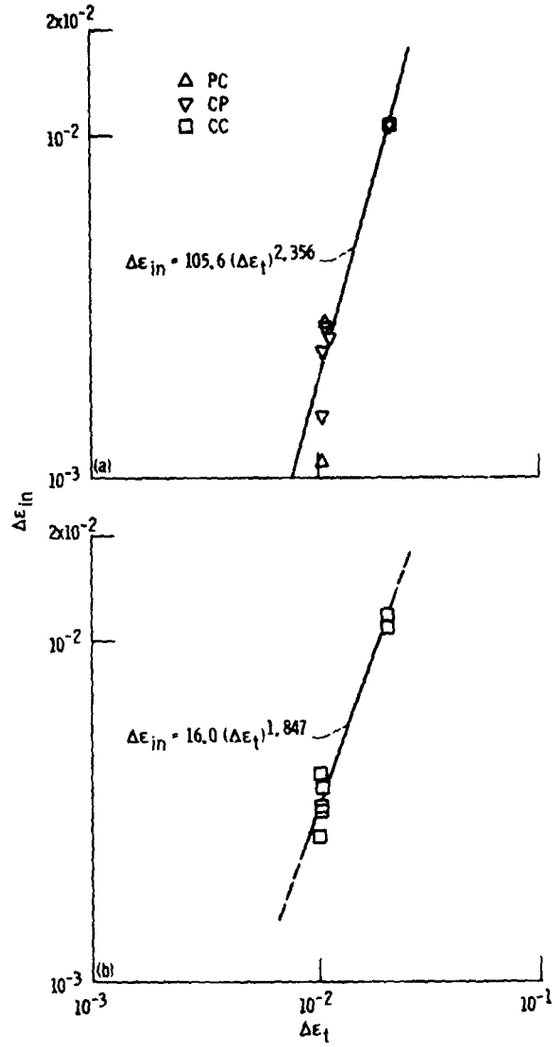

(a) PC and CP correlations.
(b) CC correlation.

Figure 34.—Relation between elastic and inelastic strain ranges for strain-hold cycles: alloy, Inconel 718; temperature, 650 °C. (Data from ref. 13, heat 6.)

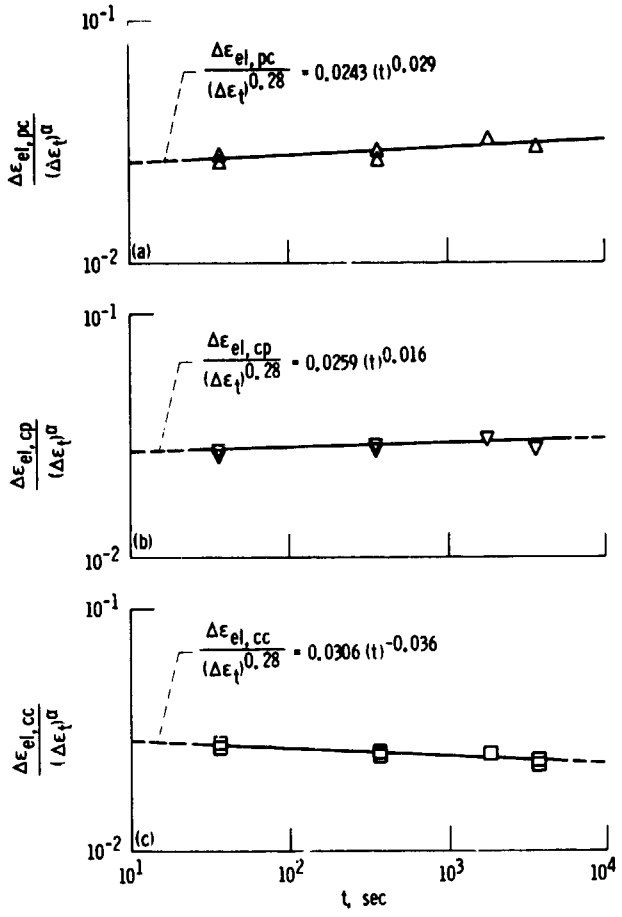

(a) PC correlation.
(b) CP correlation.
(c) CC correlation.

Figure 35.—Relation between elastic strain range and hold time for strain-hold cycles: alloy, Inconel 718; temperature, 650 °C. (Data from ref. 13, heat 6.)

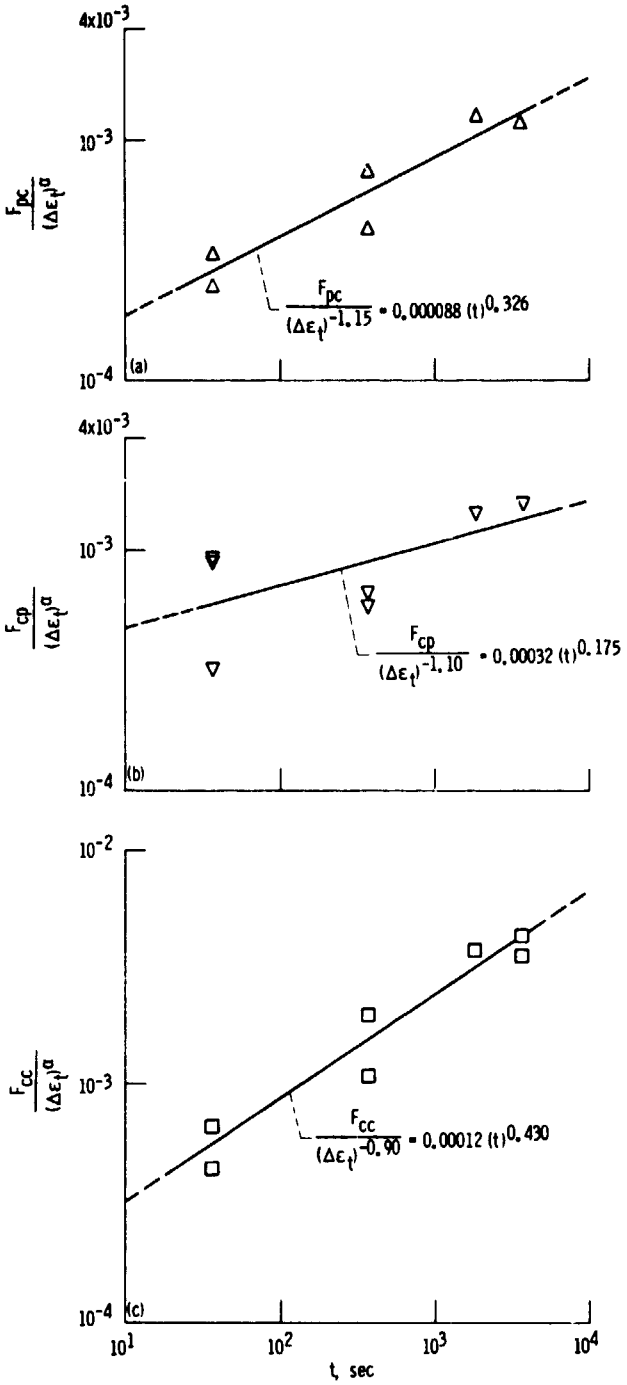

(a) PC correlation.
(b) CP correlation.
(c) CC correlation.

Figure 36.—Relation between strain fraction and hold time for strain-hold cycles: alloy, Inconel 718; temperature, 650 °C. (Data from ref. 13, heat 6.)

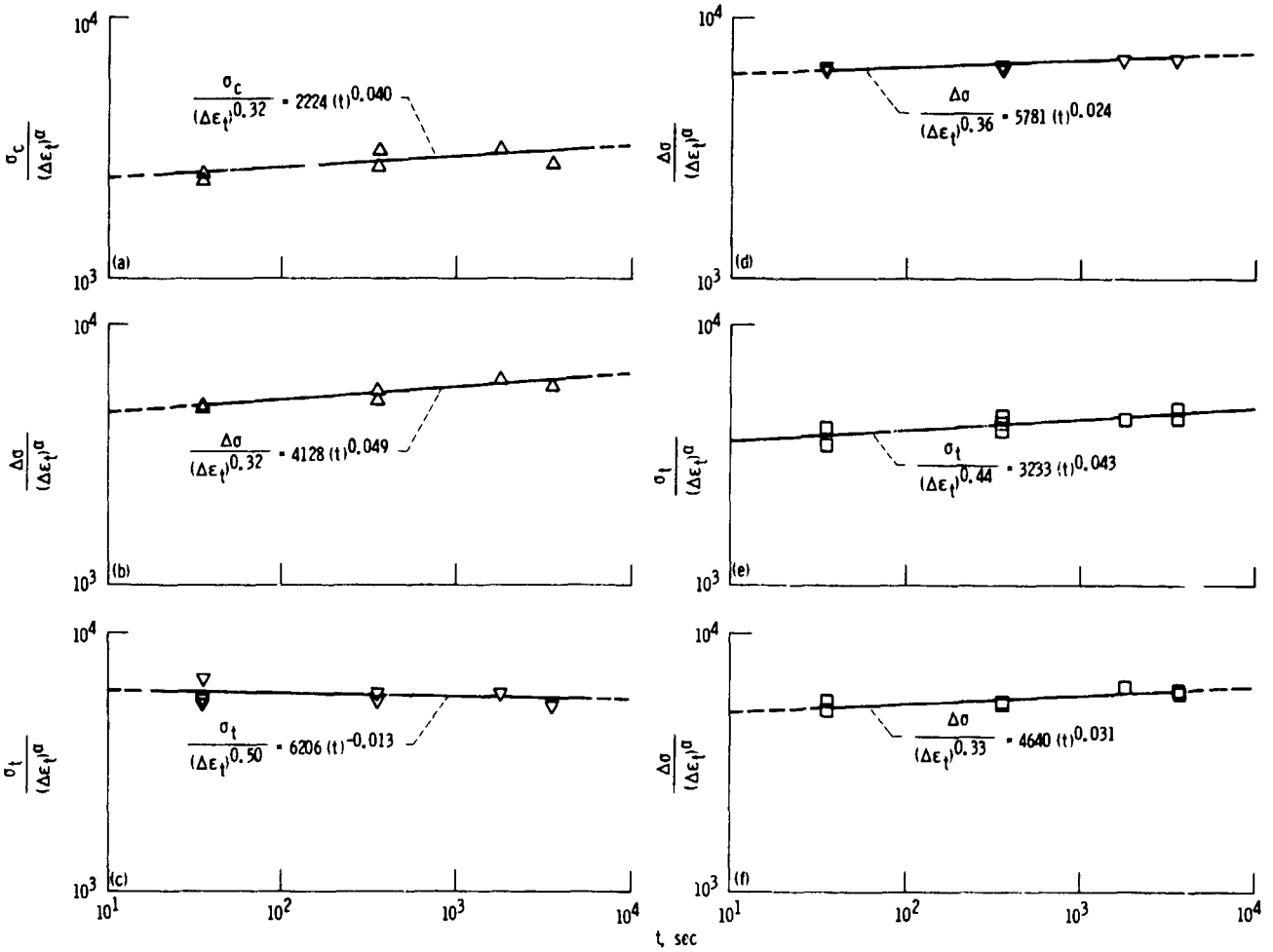

(a) PC correlation, compressive stress.
(b) PC correlation, stress range.
(c) CP correlation, tensile stress.
(d) CP correlation, stress range.
(e) CC correlation, tensile stress.
(f) CC correlation, stress range.

Figure 37.—Relation betweeen stress and hold time for strain-hold cycles: alloy, Inconel 718; temperature, 650 °C. (Data from ref. 13, heat 6.)

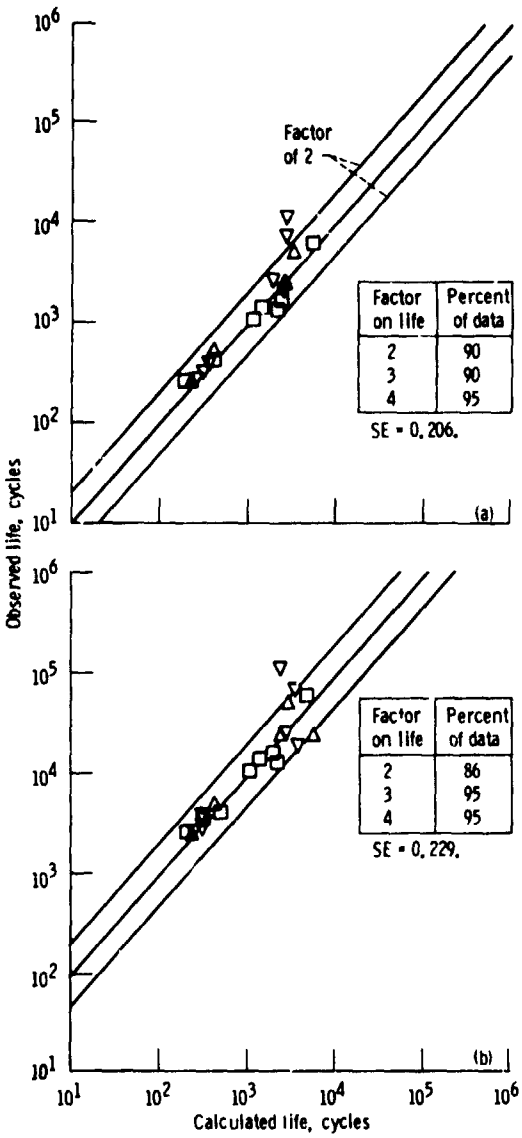

(a) Total-strain-range approach.
(b) Inelastic-strain-range approach.

Figure 38.—Life "predictions" of data used to establish strain-hold relations: alloy, Inconel 718; temperature, 650 °C. (Data from ref. 13, heat 6.)

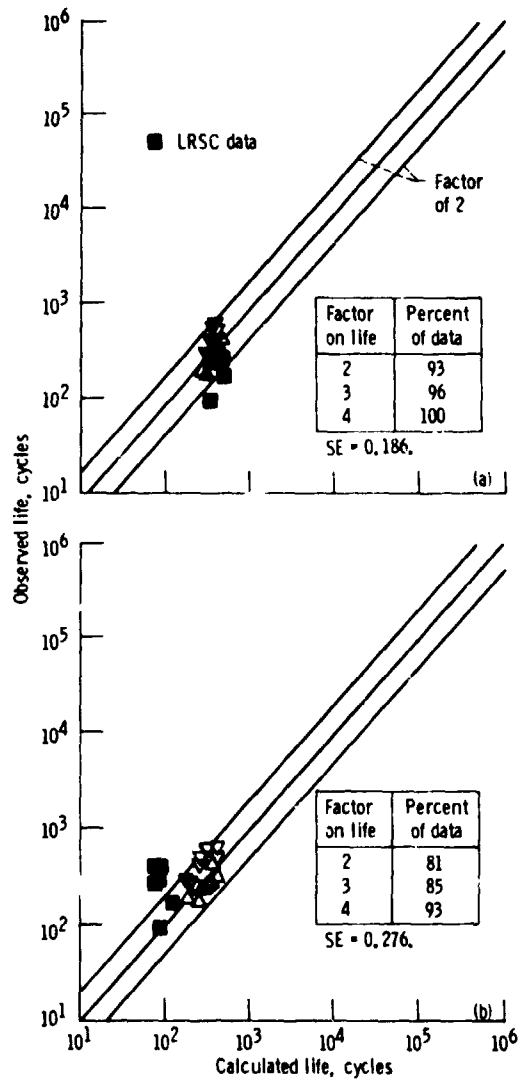

(a) Total-strain-range approach.
(b) Inelastic-strain-range approach.

Figure 39.—Life predictions of strain-hold data from reference 13 (heats 1 and 2): alloy, Inconel 718; temperature, 650 °C.

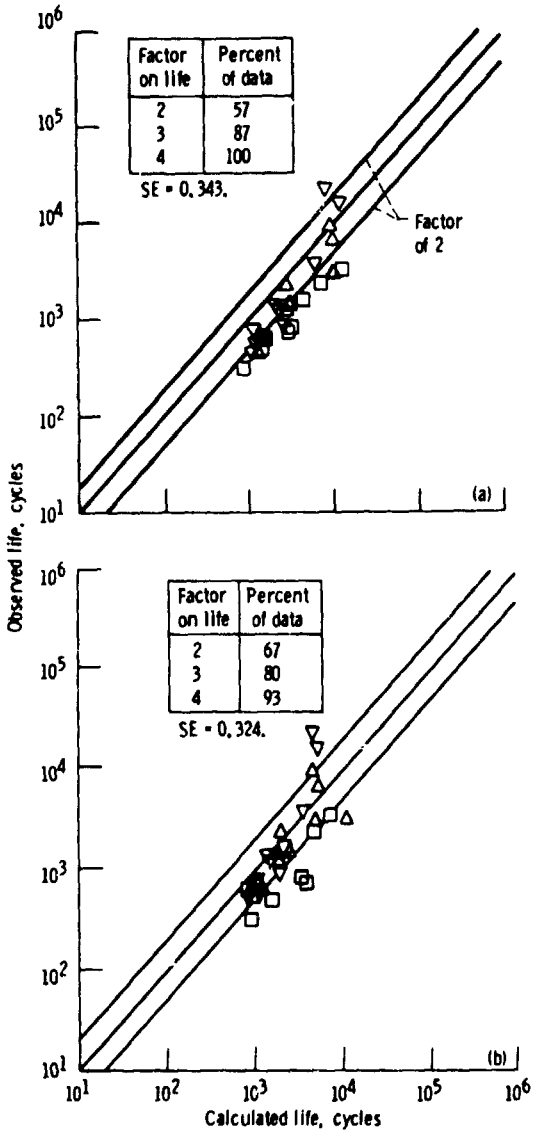

(a) Total-strain-range approach.
(b) Inelastic-strain-range approach.

Figure 40.—Life predictions of strain-hold data from reference 11: alloy, Inconel 718; temperature, 650 °C.

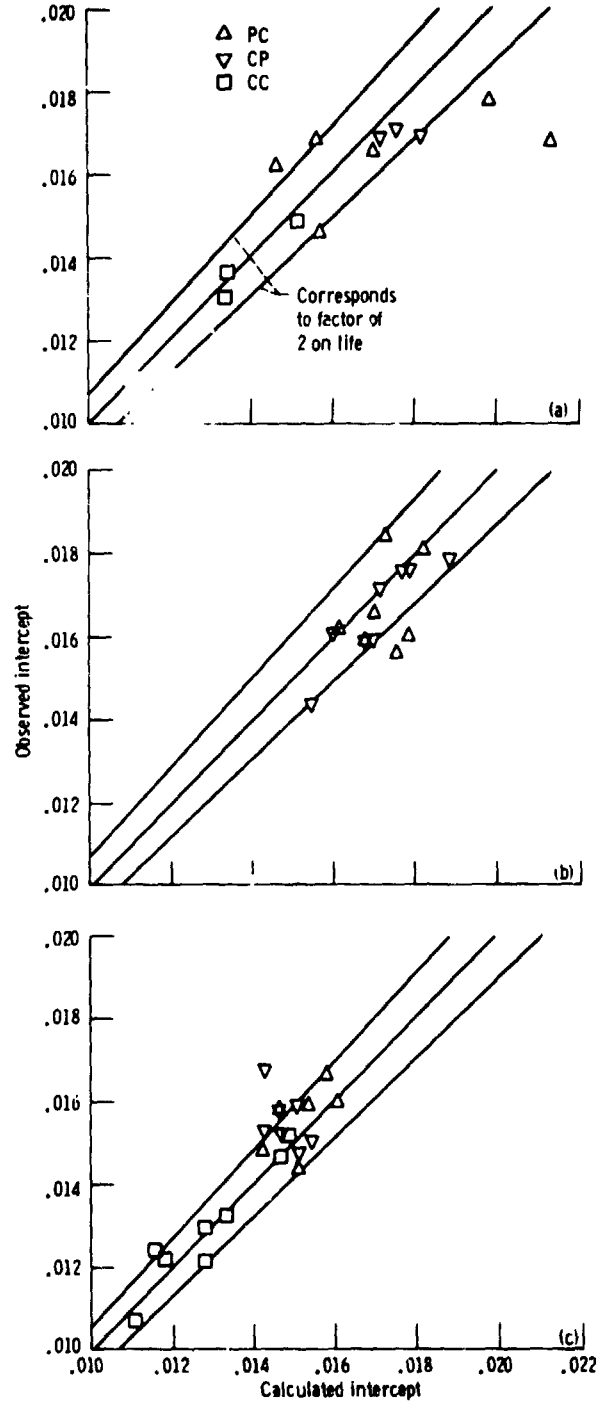

(a) Stress-hold cycles, AF2-1DA, 760 °C. (Data from ref. 8.)
(b) Strain-hold cycles, AF2-1DA, 760 °C. (Data from ref. 11.)
(c) Strain-hold cycles, Inconel 718, 650 °C. (Data from ref. 13.)

Figure 41.—Calculated versus observed values of elastic line intercept for data used to determine life and flow relations.

1. Report No.	2. Government Accession No.	3. Recipient's Catalog No.
NASA TP-2499		

4. Title and Subtitle	5. Report Date
An Update of the Total-Strain Version of SRP	October 1985
	5. Performing Organization Code 506-60-12

7. Author(s)	8. Performing Organization Report No.
James F. Saltsman and Gary R. Halford	E-.575
	10. Work Unit No.

9. Performing Organization Name and Address	11. Contract or Grant No.
National Aeronautics and Space Administration Lewis Research Center Cleveland, Ohio 44135	13. Type of Report and Period Covered Technical Paper

12. Sponsoring Agency Name and Address	14. Sponsoring Agency Code
National Aeronautics and Space Administration Washington, D.C. 20546	

15. Supplementary Notes

Similar to material presented at the Symposium on Low Cycle Fatigue - Directions for the Future, cosponsored by the American Society for Testing and Materials, the American Institute of Mining, Metallurgical and Petroleum Engineers, and the American Society for Metals, Lake George, New York, September 30 - October 4, 1985.

16. Abstract

A updated proceoure for characterizing an alloy and predicting cyclic life by using the total-strain-range version of strainrange partitioning (TS-SRP) has been developed. The principal feature of this update is a new procedure for determining the intercept of time-dependent elastic-strain-range-versus-cyclic-life lines. The procedure is based on an established relation between failure and the cyclic stress-strain response of an alloy. The stress-strain response is characterized by empirical equations presented in this report. These equations were determined with the aid of a cyclic constitutive model. The procedures presented herein reduce the testing required to characterize an alloy. Failure testing is done only in the high-strain, low-life regime; cyclic stress-strain response is determined from tests conducted in both the high- and low-strain regimes. These tests are carried out to stability of the stress-strain hysteresis loop but not to failure. Thus both the time and costs required to characterize an alloy are greatly reduced. This approach was evaluated and verified for two nickel-base superalloys, AF2-1DA and Inconel 718. The analyst can now predict cyclic life in the low-strain, long-life regime without conducting expensive failure tests in this regime or resorting to questionable extrapolations.

17. Key Words (Suggested by Author(s))	18. Distribution Statement
Fatigue (metal); Creep-fatigue; Life prediction; Strainrange partitioning; Constitutive modeling; Nickel-base superalloys; Creep; Plasticity; Strain fatigue	Unclassified - unlimited STAR Category 26

19. Security Classif. (of this report)	20. Security Classif. (of this page)	21. No. of pages	22. Price
Unclassified	Unclassified	26	A03

For sale by the National Technical Information Service, Springfield, Virginia 22161 NASA-Langley, 1985